Swept-frequency ultrasonic phase evaluation of adhesive bonding in tri-layer structures

Harold A. Haldren, Daniel F. Perey, William T. Yost, et al.

Citation: The Journal of the Acoustical Society of America **145**, 1609 (2019); doi: 10.1121/1.5094764
View online: https://doi.org/10.1121/1.5094764
View Table of Contents: https://asa.scitation.org/toc/jas/145/3
Published by the Acoustical Society of America

Swept-frequency ultrasonic phase evaluation of adhesive bonding in tri-layer structures

Harold A. Haldren,[1,a)] Daniel F. Perey,[2] William T. Yost,[2] K. Elliott Cramer,[2] and Mool C. Gupta[1]

[1]*Charles L. Brown Department of Electrical and Computer Engineering, University of Virginia, Thornton Hall, 351 McCormick Road, Charlottesville, Virginia 22904, USA*

[2]*NASA Langley Research Center, 4 Langley Boulevard, Building 1230, Mail Stop 231, Hampton, Virginia 23681, USA*

(Received 27 July 2018; revised 25 February 2019; accepted 2 March 2019; published online 28 March 2019)

As modern aerospace and automotive designs continually strive for higher performance, and thus rely on advanced composite structures where adhesive bonding is a preferred method of joining, the need for a robust quantitative nondestructive bond strength measurement method has increased. As such, advanced nondestructive evaluation methods have been researched for increased sensitivity to weak interfacial bonding and ultimately to detect "kissing" bonds. In this work, a phase-based method for interrogating bonded joints and detecting weak adhesion is developed by using swept-frequency phase measurements of ultrasonic waves reflected from an adhesive joint and modeling adhesive interfaces as a distributed spring system. The method's sensitivity to bond strength is explored by ultrasonic phase evaluation of tri-layer joints with bond quality varied by controlling ultraviolet light exposure and extracting interfacial stiffness constants of the bonds. Mechanical tensile tests found each joint failed adhesively, allowing a linear correlation to be drawn between interfacial stiffness and tensile strength, consistent with previous theoretical research. The ultrasonic phase measurement method identifies intermediate bond strengths, rather than simply detecting good or bad bonds. This technique has the potential for the verification of bond quality in lightweight aerospace and automotive designs utilizing advanced composite structures with adhesive attachments.

 https://doi.org/10.1121/1.5094764

[JFL] Pages: 1609–1618

I. INTRODUCTION

Techniques for nondestructive measurements of adhesive bond strength has been an active research area for some time. Advancements in adhesive bonding applications in aerospace and automotive design has increased the need for bond validation, as adhesive bonding is a preferred method of joining advanced composite structures and is increasingly used in aerospace design and structural repair.

While precise control of environmental conditions and the bonding process support the goal of consistent adhesion quality, inadequate surface preparation and accidental contamination still seriously degrade adhesion without being noticeable even to the trained observer or conventional inspections. Mechanical fatigue and environmental degradation reduce the strength of critical bonds, leading to their premature failure, which could lead to loss of equipment or loss of life. Thus, to certify bonded structures and verify sufficient remaining strength, it is of utmost importance to be able to nondestructively evaluate bonded joints after fabrication and during service life.

Many nondestructive evaluation (NDE) methods have been characterized on their ability to identify weak bonding and have generally proved able to detect many bonding defects such as porosity, delaminations, and complete disbonds.[1–4] However, such techniques have been unable to detect "kissing" bond regions, where adhesive and adherent are in intimate contact but unable to support the transmission of tensile and shear stresses.

The focus of most research into bonded joints has used specialized ultrasonic methods to mechanically interrogate the bonded joint on the atomic level. Several ultrasonic methods have claimed sensitivity to the quality of the adhesive/adherent interface of bonded joint (i.e., the ability of the bond to transmit stresses). These methods often make use of a modeled mass-spring system. A massless spring model for imperfect adhesion was originally proposed by Tattersall,[5] while a more fully developed model of ultrasonic interactions with imperfect interfaces included a mass-spring system derived by Baik and Thompson.[6] For many commonly encountered adhesive interfaces, including a thin array of interfacial cracks, the interfacial mass contribution is negligible. As such, a massless spring interface model has been used in several studies of adhesive bond evaluation with ultrasound. Analysis by Cantrell into adhesive bonding in alumina-epoxy[7] and carbon fiber-epoxy[8] bonded joints has related interfacial spring stiffness models to the number of intact bonds per unit area at the interface, which is directly related mechanical bond strength. Further work by Cantrell links measured amplitude and phase data from ultrasonic tone-bursts to mechanical strength at the adhesive/adherent interface via a physico-chemical model.[9]

Research into both linear[10] and modulated[11] angle beam ultrasonic spectroscopy (ABUS), supports Cantrell's analysis.

a)Electronic mail: hah5bc@virginia.edu

In ABUS, the frequency-domain characteristics of a reflected ultrasonic pulse measures the bonded joint's interfacial properties. These methods relate the shift in frequency of the amplitude minimum of both the normal and oblique incidence ultrasonic reflection coefficients of a bonded joint to the normal and shear interfacial stiffness moduli. A method developed by Nagy estimates the normal and shear interfacial stiffnesses from the characteristic frequency of the ultrasonic reflection coefficient, which is identified by the transition between low and high frequency regions of the amplitude response.[12] Additional ultrasonic techniques making use of similar normal and transverse stiffness models have been demonstrated using lamb waves,[13] shear-horizontally polarized guided waves,[14] nonlinear ultrasound,[15] a combination of compression and shear waves during adhesive cure,[16] and anisotropy observed in ultrasonic plane wave transmission coefficients.[17]

In addition to adhesive bonding, interfacial stiffness has been studied extensively by the tribology community to determine how two solid surfaces are interacting and to evaluate imperfect interfaces.[18] Similar to the adhesive/adherent interface, the solid/solid interface as distributed spring system, with the key measurement parameters being the normal and tangential interfacial stiffness. This approach to solid/solid interface quality assessment has been demonstrated with a variety of ultrasonic methods, including zero-group velocity lamb wave modes,[19] normal and angular longitudinal ultrasound,[20] and a combination of bulk and interface waves.[21] Other ultrasonic methods have used the phase response of a bonded joint to estimate adhesion quality. Królikowski and Szczepek used the pulse-echo overlap method to measure the phase of the reflection coefficient of an ultrasonic pulse in simulated kissing bonds. They found ultrasonic phase is sensitive to both interfacial stiffness and real surface area fractional contact.[22] Kissing bonds are simulated by rough surface coupons in dry-contact held together by compressional stress. Recent work into ultrasonic phase-based techniques has focused on titanium diffusion bonding quality by using double-sided[23] and single-sided[24] interrogation methods. These results also find high signal-to-noise ratio is essential, and the standard deviation of phase measurements must be small enough to adequately identify the diffusion bond as good or bad.

Despite showing some sensitivity to adhesion quality, no ultrasonic method has yet become an industry-accepted method of quantifiably measuring adhesion strength. In fact, only a few studies have shown experimentally validated correlations between measured ultrasonic data and actual mechanical strength.[17,25–28] Conventional amplitude vs time ultrasonic measurements are not sensitive enough to weak interfacial bonding and kissing bonds without gross bonding defects. Angle-beam spectroscopic ultrasonic methods show sensitivity to interface quality—especially using shear waves—yet utilize complex and time-consuming experimental setups, which makes it challenging to use in a manufacturing or repair-facility setting. Recent use of ultrasonic phase in single-interface diffusion bonds have shown excellent interfacial stiffness sensitivity; however, the high signal-to-noise ratio required for interface characterization are, in many cases, difficult to obtain with broadband pulse analysis.

In this work, an ultrasonic adhesion quality measurement method is demonstrated, by combining the advantages of frequency-based with phase-based ultrasonic methods, while overcoming some of the challenges of previous techniques. This method uses a tone-burst from a constant frequency pulsed phase-locked-loop (CFPPLL) instrument to measure the phase of a constant frequency—rather than broadband—ultrasonic pulse.[29] By measuring ultrasonic phase at a single frequency and using narrowband filtering to suppress noise, high signal-to-noise ratios and consequently, low phase measurement noise, is obtained with commercially available damped transducers. By sweeping the frequency over a desired range and correcting for transducer phase response, a high-resolution ultrasonic phase vs frequency spectrum—as opposed to the amplitude spectrum used in many previous studies—is obtained for characterization of adhesion quality. This method has advantages over amplitude-based techniques, by being insensitive to attenuation changes and other amplitude-based sources of uncertainty (such as surface roughness).

The swept-frequency ultrasonic phase measurement method is used to examine adhesive bonding properties of tri-layered bonded joints near their acoustic resonance, using polished glass adherents where the degree of adhesion is varied by exposure to ultraviolet (UV) light. To distinguish between adhesive and cohesive properties in the bonded joint, changes in elastic modulus of the adhesive layer during cure are measured using a broadband pulse-echo time-of-flight technique. The sound velocity at a UV-light exposure time is then used in an inverse algorithm for determining interfacial stiffness from the measured phase spectrum of the bondline reflection. Finally, ultrasonically measured interfacial stiffness values are correlated to destructive mechanical testing results.

II. THEORY

Starting with quasi-static model for ultrasonic interactions with imperfect interfaces developed by Baik and Thompson,[6] the normal-incidence particle displacement wave reflection coefficient from imperfect bonding within a tri-layer adhesive joint is found. An ultrasonic particle displacement plane wave is excited into the bondline at a normal incidence, represented by Eq. (1), where T_i is the wave amplitude, $i = \sqrt{-1}$, ω is angular frequency, t is time, k_1 is the complex wavenumber in the incident medium, and x is the distance travelled by the wave

$$u_i(x,t) = T_i e^{i(\omega t - k_1 x)}. \tag{1}$$

Using the tri-layer configuration in Fig. 1, the incident ultrasonic plane wave amplitude transmitted into the bondline, T_i, is assumed to be unity for simplicity. For the purposes of this derivation, the Adherent 1 and 2 media are assumed semi-infinite half spaces and only the area around the adhesive bondline is considered. Interfacial adhesive bond quality is represented by the distributed mass-spring system defined by Baik and Thompson, with stiffness per unit area constants K_1 and K_2—also referred to as the spring constant flux—and mass per unit area m_1 and m_2 at each adhesive/adherent interface.[6]

In Fig. 1, x is the distance from the first adherent interface, L_{BL} is the bondline thickness, R_{adh} and T_{adh} are, respectively, the reflection and transmission coefficients within the adhesive, T_o is the ultrasonic transmission coefficient through the bondline, and R_{BL} is the bondline reflection coefficient. The reflected particle displacement waves within the bondline are separated by a time-of-flight (ToF) of $2L_{BL}/c_{adh}$, where c_{adh} is the sound velocity within the adhesive. Assuming the adhesive ToF is small with respect to the incident tone-burst duration, the net effect of multiple decaying reflections within the bondline is considered.

The ultrasonic reflection coefficient of the tri-layer structure with two imperfect interfaces is found by applying the appropriate boundary conditions at each interface and simultaneously solving coupled equations for the bondline particle displacement wave reflection coefficient, R_{BL}. Table I shows the assumed ultrasonic displacement and stress equations in each medium as a function of position. The time dependence portion of the equations is omitted throughout this derivation. The ultrasonic stress was found from the displacement equations from the relation, $\sigma = E\,\partial u/\partial x$, where u is ultrasonic displacement, x is position, σ is stress, and E is the longitudinal elastic modulus. The longitudinal elastic modulus used here is defined as $E = \lambda + 2G = \rho c^2$, where λ is Lamé's first parameter, G is the shear modulus, ρ is the mass density, and c is the sound velocity within the medium.

In Table I, $k_n = \omega/c_n + i\alpha_n$ is the complex ultrasonic wavenumber in each medium given input angular frequency ω, sound velocity c_n, and acoustic attenuation coefficient α_n; and $E_n = \rho_n c_n^2$ is the longitudinal elastic modulus in each medium given mass density ρ_n and sound velocity. While the attenuation coefficient is nominally frequency dependent, it is assumed constant in this work, as small frequency ranges are used. The imperfect interface boundary conditions from Baik and Thompson[6] are applied to each interface; the results are given in Table II.

After applying each of the four boundary conditions in Table I to the displacement and stress equations from Table II, the resulting system of equations was written in terms of the four unknown reflection and transmission coefficients, displayed in matrix form in Eq. (2),

$$
\begin{aligned}
&Ay = b \quad A = \begin{bmatrix} A_1 & A_2 & A_3 & A_4 \end{bmatrix},\\
&A_1 = \begin{bmatrix} 2K_1 + iE_1k_1 \\ -m_1\omega^2 + 2iE_1k_1 \\ 0 \\ 0 \end{bmatrix},\\
&A_2 = \begin{bmatrix} -2K_1 + iE_{adh}k_{adh} \\ -m_1\omega^2 - 2iE_{adh}k_{adh} \\ (2K_2 + iE_{adh}k_{adh})e^{iL_{BL}k_{adh}} \\ (-m_2\omega^2 + 2iE_{adh}k_{adh})e^{iL_{BL}k_{adh}} \end{bmatrix},\\
&A_3 = \begin{bmatrix} -2K_1 - iE_{adh}k_{adh} \\ -m_1\omega^2 + 2iE_{adh}k_{adh} \\ (2K_2 - iE_{adh}k_{adh})e^{-iL_{BL}k_{adh}} \\ (-m_2\omega^2 - 2iE_{adh}k_{adh})e^{-iL_{BL}k_{adh}} \end{bmatrix},\\
&A_4 = \begin{bmatrix} 0 \\ 0 \\ -2K_2 - iE_2k_2 \\ -m_2\omega^2 + 2iE_2k_2 \end{bmatrix}, \quad y = \begin{bmatrix} R_{BL} \\ R_{adh} \\ T_{adh} \\ T_o \end{bmatrix},\\
&b = \begin{bmatrix} -2K_1 + iE_1k_1 \\ m_1\omega^2 + 2iE_1k_1 \\ 0 \\ 0 \end{bmatrix}.
\end{aligned}
\tag{2}
$$

The coupled system in Eq. (2) is solved by the inverse matrix method to find a closed-form solution for R_{BL}. After simplification, omitted here for brevity, the bondline reflection coefficient is displayed in Eq. (3),

$$
\begin{aligned}
&R_{BL} = \frac{C_N\cos(k_{adh}L_{BL}) + iS_N\sin(k_{adh}L_{BL})}{C_D\cos(k_{adh}L_{BL}) + iS_D\sin(k_{adh}L_{BL})},\\
&C_N = G_{adh}\left[(G_1 - G_2)F + \frac{4}{K_e}\left(\frac{4G_1G_2}{m_1m_2} - \omega^4\right) - \frac{4\omega^2}{m_e}\left(\frac{G_1G_2}{K_1K_2} - 4\right) - 16\omega^2\left(\frac{G_1}{K_1m_1} - \frac{G_2}{K_2m_2}\right)\right],\\
&C_D = G_{adh}\left[(G_1 + G_2)F + \frac{4}{K_e}\left(\frac{4G_1G_2}{m_1m_2} + \omega^4\right) - \frac{4\omega^2}{m_e}\left(\frac{G_1G_2}{K_1K_2} + 4\right) - 16\omega^2\left(\frac{G_1}{K_1m_1} + \frac{G_1}{K_2m_2}\right)\right],\\
&S_N = \left(G_1G_2 - G_{adh}^2\right)F + 4\left(\frac{G_1}{K_1} - \frac{G_2}{K_2}\right)\left(\frac{4G_{adh}^2}{m_1m_2} + \omega^4\right) - 4\omega^2\left(\frac{G_1}{m_1} - \frac{G_2}{m_2}\right)\left(\frac{G_{adh}^2}{K_1K_2} + 4\right) + 16\left(\frac{G_{adh}^2G_1G_2}{K_1K_2m_1m_2} - \omega^4\right),\\
&S_D = \left(G_1G_2 + G_{adh}^2\right)F + 4\left(\frac{G_1}{K_1} + \frac{G_2}{K_2}\right)\left(\frac{4G_{adh}^2}{m_1m_2} + \omega^4\right) - 4\omega^2\left(\frac{G_1}{m_1} + \frac{G_2}{m_2}\right)\left(\frac{G_{adh}^2}{K_1K_2} + 4\right) + 16\left(\frac{G_{adh}^2G_1G_2}{K_1K_2m_1m_2} + \omega^4\right),\\
&F = \frac{16}{m_1m_2} + \frac{\omega^4}{K_1K_2} - 4\omega^2\left(\frac{1}{K_2m_1} + \frac{1}{K_1m_2}\right), \quad G_1 = iE_1k_1,\ G_2 = iE_2k_2,\\
&G_{adh} = iE_{adh}k_{adh}, \quad K_e = \left(K_1^{-1} + K_2^{-1}\right)^{-1},\ m_e = \left(m_1^{-1} + m_2^{-1}\right)^{-1}.
\end{aligned}
\tag{3}
$$

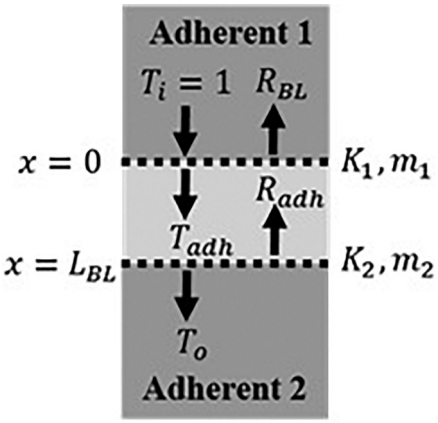

FIG. 1. Normal-incidence ultrasonic reflections within thin-adhesive tri-layer structure.

While Eq. (3) is useful in modeling the theoretical ultrasonic amplitude or phase response of nearly any given tri-layer material system, the complexity of the reflection coefficient can be simplified in many common situations. In this work, the same material is used for both upper and lower adherent. Also, no modification or contamination is added to either adhesive/adherent interface to cause them to have different bond strengths, so it is assumed both interfaces have the same properties and should not have interfacial inclusions or cracks. Under these conditions, the stiffness constants at each interface are assumed to be equal and the interfacial mass at each interface is zero. Under the assumptions $E_1 = E_2$, $k_1 = k_2$, $K_1 = K_2 = K$, and $m_1 = m_2 = 0\,\mathrm{kg/m^2}$, R_{BL} keeps the same form as shown in Eq. (3), but the coefficients in front of the hyperbolic cosine and sine terms are simplified

$$
\begin{aligned}
R_{BL} &\approx \frac{C_N \cos(k_{adh}L_{BL}) + iS_N \sin(k_{adh}L_{BL})}{C_D \cos(k_{adh}L_{BL}) + iS_D \sin(k_{adh}L_{BL})},\\
C_N &\approx \frac{2G_1^2 G_{adh}}{K},\\
C_D &\approx 2G_1 G_{adh}\left(1 + \frac{G_1}{K}\right),\\
S_N &\approx G_1^2 - G_{adh}^2 + \frac{G_1^2 G_{adh}^2}{K^2},\\
S_D &\approx G_1^2 + G_{adh}^2 + \frac{G_1 G_{adh}^2}{K}\left(2 + \frac{G_1}{K}\right).
\end{aligned}
\tag{4}
$$

Of particular interest in this work is the frequency range surrounding the ultrasonic anti-resonance frequency (f_{ar}) of bondline reflections. Assuming perfect interfacial bonding, ultrasonic anti-resonance of the reflection coefficient occurs when the bondline thickness is one half wavelength thick, corresponding to $f_{ar} = c_{adh}/2L_{BL}$. At the anti-resonance frequency, the amplitude of R_{BL} attains a local minimum and the phase of R_{BL} undergoes an inversion from negative to positive values. However, weak bonding at the adhesive/adherent interface causes a shift of the anti-resonance frequency, as well. This effect can be thought of as the stiffness of the interfaces slightly changing the effective stiffness of the entire adhesive layer, including its interfaces. The complex reflection coefficient in Eq. (4) is used to model the phase vs frequency response of bondline reflection coefficient to extract unknown adhesive bonding parameters. The amplitude and phase spectra are computed for a given set of material properties by expressing R_{BL} in polar form as a function of input acoustic frequency (i.e., $R_{BL}(f) = |R_{BL}(f)|e^{i\phi(f)}$).

TABLE I. Ultrasonic wave displacement and stress equations in each medium.

Medium (subscript)	Displacement	Stress
Adherent (1)	$u_1(x) = e^{-ik_1 x} + R_{BL}\, e^{ik_1 x}$	$\sigma_1(x) = -iE_1k_1 \times (e^{-ik_1 x} - R_1 e^{ik_1 x})$
Adhesive (adh)	$u_{adh}(x) = T_{adh}e^{-ik_{adh}x} + R_{adh}e^{ik_{adh}x}$	$\sigma_{adh}(x) = -iE_{adh}k_{adh} \times (T_{adh}e^{-ik_{adh}x} - R_{adh}e^{ik_{adh}x})$
Adherent (2)	$u_2(x) = T_o e^{-ik_2(x-L_{BL})}$	$\sigma_2(x) = -iE_2k_2T_o e^{-ik_2(x-L_{BL})}$

III. EXPERIMENTAL

To investigate the ability of swept-frequency phase measurements to interrogate adhesive properties, several sets of experiments were performed. Idealized lap joints made with smooth glass adherents were chosen to minimize experimental uncertainty arising from surface roughness and internal ultrasonic scattering in these initial experiments. Transparent adherents also permit visual inspection of bonding defects and allow for the use of adhesives curable with UV light. By varying the exposure time to UV light, the adhesive and cohesive properties of the lap joint can be precisely controlled without the need for high temperatures, allowing for *in situ* adhesive bond evaluation with commercial ultrasonic transducers.

Schott Borofloat® 33 glass cut into 5.08 cm wide × 5.08 cm long × 1.10 cm thick coupons were purchased from the S. I. Howard Glass Company to be used as adherents. The glass coupons were bonded together with Norland Optical Adhesive (NOA) 60, a UV-curable adhesive, obtained from Norland Products Inc. NOA 60 does not continue to cure at room temperature when not exposed to UV light, allowing for correlation between ultrasonically and mechanically evaluated bond strengths without a change in degree-of-cure.

Prior to bonding, each glass coupon was cleaned with an ethanol wipe, a 60 min ultrasonic cleaning bath in reagent grade ethanol, and vapor degreasing with ethanol. After

TABLE II. Imperfect interface boundary conditions in tri-layer model.

Interface	Interfacial stiffness boundary condition	Interfacial mass boundary condition
Upper adherent - adhesive (x = 0)	$\sigma_1(0) + \sigma_{adh}(0) = 2K_1(u_{adh}(0) - u_1(0))$	$-m_1\omega^2(u_{adh}(0) + u_1(0)) = 2(\sigma_{adh}(0) - \sigma_1(0))$
Lower adhesive - adherent ($x = L_{BL}$)	$\sigma_{adh}(L_{BL}) + \sigma_2(L_{BL}) = 2K_2(u_2(L_{BL}) - u_{adh}(L_{BL}))$	$-m_2\omega^2(u_2(L_{BL}) + u_{adh}(L_{BL})) = 2(\sigma_2(L_{BL}) - \sigma_{adh}(L_{BL}))$

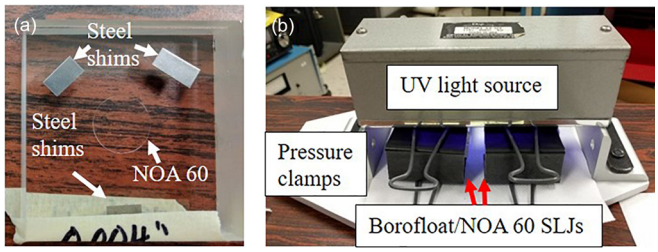

FIG. 2. (Color online) (a) Post-cure image of Borofloat/NOA 60 single lap joint; (b) UV light curing setup for bonded joints.

drying, a single drop of room-temperature NOA 60 was applied to one of the adherents. Three small pieces of stainless steel shim stock were then placed on the adherent to hold a uniform bondline thickness between joints. The shim stock thickness was 204 μm for the sound velocity measurement experiment and 102 μm for the adhesive bond evaluation experiments. Next, a second glass adherent was placed on top of the other to form a single lap joint. Two 2.54 cm thick clamps on opposite sides of the joint held the thickness during cure. In each specimen, a dial micrometer was used to measure the adherent thicknesses before cure and lap joint thickness after cure to determine the bondline thickness. An example image of a fully cured lap joint is shown in Fig. 2(a).

The joints were placed under a UV light source to cure, as shown in Fig. 2(b). NOA 60 cures optimally via UV light with wavelengths of 350–380 nm and requires about 3 J/cm^2 of energy for full cure, according to Norland Products, Inc. The UV light source is a 5.08 cm × 15.24 cm model 22-UV manufactured by Optical Engineering, Inc (now manufactured by Macken Instruments, Inc.) and uses a low-pressure mercury florescent bulb with UV phosphor and blue tinted glass to suppress visible emission. The source emits light with a maximum intensity of 5 mW/cm^2 and wavelengths primarily between 340 and 390 nm, with peak emission at 360 nm, according to the manufacturer. The transmission spectrum of Schott Borofloat® 33 is only given by the manufacturer for thicknesses up to 5 mm but is assumed to be ~80% in the 350–380 nm range. Assuming an intensity of 2.5 mW/cm^2 in the 350–380 nm range reaches the top of the adherent and 80% transmission through the adherent, it is conservatively estimated that a cure time of 25 min is required to fully cure the adhesive with 3 J/cm^2 of energy.

A. Sound velocity measurements via ultrasonic time-of-flight

As both sound velocity and interfacial stiffness flux shift the frequency of anti-resonance of ultrasonic bondline reflections, it is necessary to independently determine the adhesive sound velocity as a function of cure. A 12.7 mm diameter, nominally 50 MHz damped ultrasonic transducer (model V214BA from Olympus) was adhered under a Borofloat glass/NOA 60 lap joint with Sono 600 ultrasonic couplant (obtained from Magnaflux) during cure. The shim thickness was made to easily separate ultrasonic reflections coming from each interface within the bondline.

At 27 different time intervals within cure process, the UV light source was blocked and the bonded joint was evaluated with a broadband ultrasonic pulse from a GE Panametrics Model 5900PR pulser-receiver. The time-of-flight between consecutive reflections within the bondline was measured with a LeCroy WaveRunner 6200 oscilloscope. The broadband pulse had a passband of 1 kHz–200 MHz and a pulse energy of 1 μJ. The reflected signal was amplified by 38 dB prior to viewing on the oscilloscope.

B. *In situ* ultrasonic bonding evaluation during cure

A glass/UV-curable adhesive lap joint was fabricated and ultrasonically evaluated *in situ* throughout its cure process. A 6.35 mm diameter, broadband Olympus V112 ultrasonic transducer was mounted underneath the bonded joint during cure and was coupled into the bottom adherent with Sono 600 ultrasonic couplant.

At different time intervals throughout the cure process, the UV light source was blocked so that swept-frequency phase measurements were made with the CFPPLL instrument.[29] The phase of the first reflection from the bondline was measured as a function of frequency. As the adhesive layer is thin with respect to the acoustic tone-burst duration, multiple reflections from inside the adhesive layer are combined within the received tone-burst. The ultrasonic driving frequency was swept in 0.01 MHz increments through the 8.5–11.75 MHz range. Using the CFPPLL instrument to provide the same input phase offset used in the bondline reflection measurement, a reference phase vs frequency measurement was obtained from the first back-wall reflection of an unbonded section of the lower glass adherent. This measurement is used to account for the phase response caused by the adherent, instrumentation, ultrasonic transducer, and ultrasonic couplant.

C. Post-cure ultrasonic and mechanical bonding evaluation

To correlate ultrasonic measurements with mechanical bond strength, a set of ten Borofloat/NOA 60 bonded joints were fabricated with UV-light exposure times varying from 3 to 60 min. The diameter of the circular adhesive cross-section was determined to a tolerance of ±1 mm

In this study, a load cell and screw clamp were placed in-line with the lap joint/transducer setup, providing a compressive bias of ~178 N to the transducer during each measurement. Ultrasound is coupled into the adherent of the joint under test via Sono 600 ultrasonic couplant. In this setup, the phase of the first reflection from the bondline of each bonded joint was evaluated with the CFPPLL instrument through the 8.5–11.75 MHz range with an Olympus V112 transducer.[29] A reference phase vs frequency measurement was also obtained from the first back-wall reflection of an unbonded section of the structure, using the same load-cell, compressive bias, and ultrasonic phase offset. The purpose of the reference measurement is to later subtract out the phase spectra due to the adherent, instrumentation, ultrasonic transducer, and ultrasonic couplant layer.

After ultrasonic testing, metal angle brackets and sheet stock were bonded to the lap joints with room-temperature-curing Hysol 9394 epoxy, as shown in Fig. 3(a). Spring-based clamps applied pressure during cure. The metal sheets on each end of the structure were placed within the grips of an MTS Alliance RT/100 load frame during mechanical tensile testing, as shown in Fig. 3(b). Each bonded joint was pull-tested where a constant load rate of 267 N/min was applied until failure.

IV. RESULTS AND DISCUSSION

A. Sound velocity measurements via ultrasonic time-of-flight

The amplitude vs time responses from ultrasonic pulse reflections within the bondline were examined as a function of UV-light exposure. Bondline reflection measurements from several different degrees of cure are plotted in Fig. 4, which shows three typical measured response curves. A trend is observed of the peak amplitude of the second reflection to decreasing in time as a function of cure.

The ToF of each pulse within the bondline was found by taking the difference in time of maximum amplitude between the first and second bondline reflections. The lap joint's bondline thickness is $206.6 \pm 3.6\,\mu$m. Adhesive longitudinal wave velocity was calculated. The measured ToF within the bondline and the computed adhesive longitudinal wave velocity are plotted in Fig. 5. The velocity measurements are used later in modeling the ultrasonic phase and amplitude vs frequency responses of the bondline as a function of UV light exposure. Additional velocity measurements may not be necessary to measure interfacial stiffness flux in applications where the adhesive properties are well-known and the cure-cycle is well controlled.

B. *In situ* ultrasonic bonding evaluation during cure

To obtain the phase vs frequency response of only the adhesive bondline reflection coefficient, the measured reference phase from the back-wall of the unbonded adherent is subtracted from the measured phase from the tri-layer structure at each UV-exposure time. For displacement waves, the acoustic reflection coefficient for a glass/air interface can be simply modeled as $R_{glass/air} = (Z_{glass} - Z_{air})/(Z_{glass} + Z_{air})$, where Z_{glass} and Z_{air} are the acoustic impedances of glass and air, respectively. Near 20 °C, air has an acoustic impedance of $Z_{air} = 415$ Rayl,[30] whereas the glass used in this work has a measured acoustic impedance of $Z_{glass} = 12.3 \times 10^6$ Rayl. As a result, $R_{glass/air} \approx 1$, and the phase shift at the glass/air interface at the back-wall of the unbonded adherent is zero. This makes it straightforward to subtract out the measured reference phase to obtain the phase of the bondline reflection coefficient.

The total measured reference phase from the back-wall of the adherent is expressed in Eq. (5), where $\phi_{adherent}(f)$ is the phase shift caused acoustic waves traveling through the adherent, $\phi_{trans}(f)$ is the phase response of the transducer, $\phi_{instr}(f)$ is the phase response of the CFPPLL instrumentation, and $\phi_{coup}(f)$ is the phase shift caused by acoustic waves traveling through the transducer/couplant/adherent interface when being transmitted and received

$$\phi^{meas}_{adherent}(f) = \phi_{adherent}(f) + \phi_{trans}(f) + \phi_{instr}(f) + \phi_{coup}(f). \quad (5)$$

Equation (6) describes the measured phase vs frequency response of the first reflection from the adherent/adhesive/

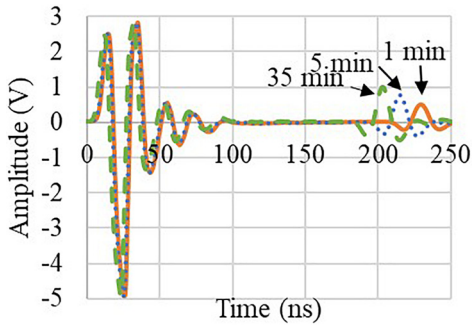

FIG. 4. (Color online) Selected ultrasonic pulse reflections from bondline with different UV-light exposure times: 1 min (solid orange), 5 min (dotted blue), 35 min (dashed green).

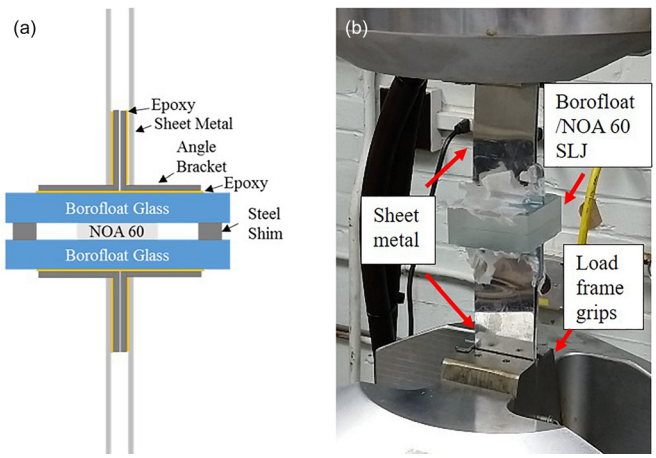

FIG. 3. (Color online) (a) Tensile testing structural arrangement for Borofloat/NOA 60 lap joints; (b) Image of Borofloat/NOA 60 joint within grips of load frame.

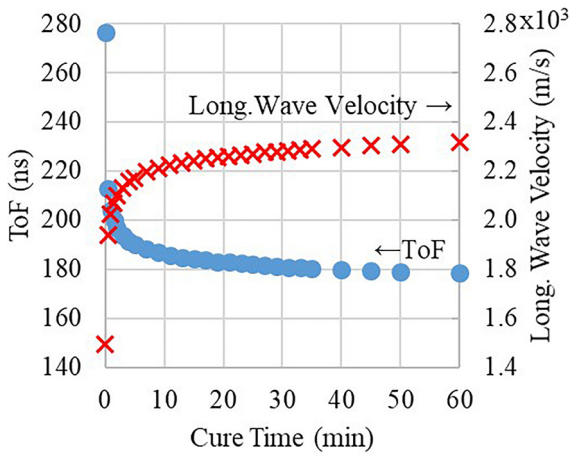

FIG. 5. (Color online) Measured time-of-flight of ultrasonic pulses within bondline (blue dots) and calculated longitudinal wave velocity (red crosses) vs adhesive UV light exposure time.

adherent interface in the tri-layer structure, where $\phi_{R_{BL}}(f)$ is the phase response of the bondline reflection coefficient and $\phi_{diff}(f)$ accounts for unknown phase shifts caused by differences in the adherent material properties and thickness between measurement points as well as differences in acoustic couplant thickness between tests

$$\phi^{meas}_{tri-layer}(f) = \phi_{adherent}(f) + \phi_{R_{BL}}(f) + \phi_{trans}(f) + \phi_{instr}(f) + \phi_{coup}(f) + \phi_{diff}(f). \quad (6)$$

By subtracting $\phi^{meas}_{adherent}(f)$ from $\phi^{meas}_{tri-layer}(f)$, the result is primarily the phase of the bondline reflection coefficient. This new phase, hereafter referred to as the measured phase response of the adhesive bondline, is expressed in Eq. (7). The unknown phase shifts encompassed by $\phi_{diff}(f)$ should be relatively small, as the smooth glass adherents used in this study are quite uniform in both composition and thickness. Additionally, care is taken to avoid variations in acoustic couplant thickness by providing a consistent compressive load to the transducer across ultrasonic tests. The resulting bondline phase responses at selected cure times are displayed in Fig. 6,

$$\phi^{meas}_{BL}(f) = \phi^{meas}_{tri-layer}(f) - \phi^{meas}_{adherent}(f) = \phi_{R_{BL}}(f) + \phi_{diff}(f). \quad (7)$$

Of note from Fig. 6 is the increase in the anti-resonance frequency (f_{ar})—where the phase inversion occurs—with increased cure. This frequency increase is thought to be caused by the adhesive stiffening due to polymer cross-linking during cure, causing a sound velocity increase. Additionally, the "sharpness" of the phase inversion or the slope of phase shift ($d\phi/df$) at f_{ar} increases with cure, due to decreasing bulk adhesive attenuation. The decrease in adhesive attenuation as a function of cure was also seen in the ToF measurements taken with 50 MHz pulses in the adhesive. It is thought the decreasing adhesive attenuation

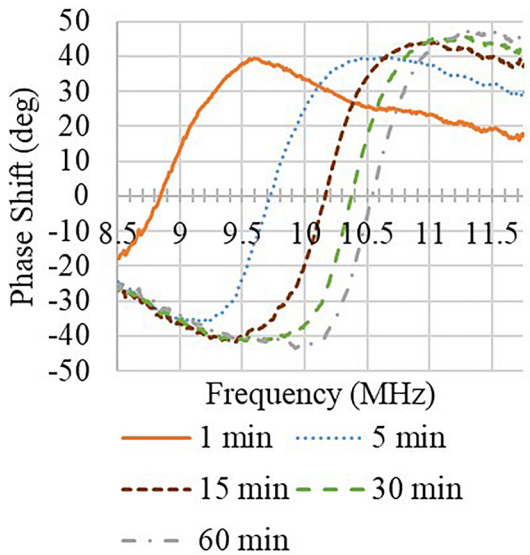

FIG. 6. (Color online) Phase vs frequency responses of bondline reflections, $\phi^{meas}_{BL}(f)$, for selected cure times of *in situ* monitored bonded joint.

TABLE III. Set parameters in model of phase of ultrasonic reflection coefficient of bondline.

Parameter	Value
Adherent sound vel.: c_1	5640 m/s
Adhesive sound vel.: c_{adh}	1500–2400 m/s
Adherent density: ρ_1	2180 kg/m^3
Adhesive density: ρ_{adh}	1290 kg/m^3
Bondline thickness: L_{BL}	108.3 μm

coefficient is caused by polymer cross-linking during cure, which decreases ultrasonic absorption within the adhesive.

To solve the inverse problem of obtaining the unknown properties of acoustic attenuation in the adhesive layer and interfacial stiffness, a curve-fitting model was developed using the robust least absolute residual fitting algorithm. In this model, described by Eq. (8), the measured phase response of the bondline, $\phi^{meas}_{BL}(f)$ is fit to the theoretical phase of the bondline reflection coefficient plus a linear term to account for small differences in adherent thickness or material properties as well as couplant thickness variations

$$\phi_{model}(f;K,\alpha_{adh},a,b) = \phi^{theor}_{R_{BL}}(f;K,\alpha_{adh}) + af + b. \quad (8)$$

In Eq. (8), the input frequency f is the independent variable, $\phi^{theor}_{R_{BL}}$ is the theoretical phase of the bondline reflection coefficient described by Eq. (4), and a and b are some real numbers. Table III shows the set constant parameters used in the curve fitting method for the phase response: c_1, ρ_1, ρ_{adh}, and L_{BL}. The lap joint's bondline thickness is measured to be 108.3 ± 3.1 μm. The only set parameter which changes is the adhesive sound velocity, c_{adh}, which was measured for each UV-light exposure time and accounts for the stiffening of the adhesive during cure (i.e., increasing E_{adh}). Adherent and adhesive mass densities were obtained from manufacture specifications. Only K, α_{adh}, a, b are free to change in order to the measured phase data to the model. The initial guess, lower bound, and upper bound for each free parameter used in the model is shown in Table IV. Figure 7 shows an example of the curve-of-best-fit found for the phase response of the bondline after 30 min of cure.

From the curve fitting of the phase response in the 8.5–11.75 MHz range, the interfacial stiffness per unit area coefficients between the adhesive and adherent as well as the adhesive attenuation coefficient were extracted as a function of cure time and are plotted in Fig. 8. 95% confidence bounds were also found for the two parameters from the curve fits, but they are not plotted in Fig. 8 as they are too

TABLE IV. Free parameters in model of phase of ultrasonic reflection coefficient of bondline.

Parameter (units)	Initial guess	Lower bound	Upper bound
Adhesive attenuation: α_{adh} (Np/m)	1000	0	10,000
Interfacial stiffness flux: K (N/m^3)	10^{16}	10^{12}	10^{20}
Linear term: a (deg/Hz)	0	-3×10^{-6}	3×10^{-6}
Constant term: b (deg)	0	−10	10

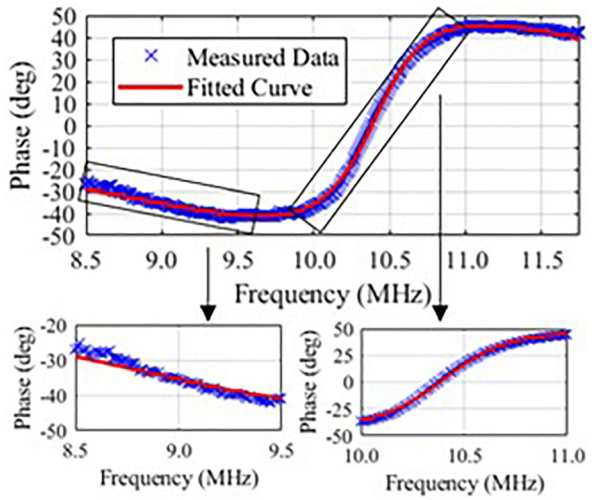

FIG. 7. (Color online) Curve fit of $\phi_{BL}^{meas}(f)$ from 30 min cured joint.

small to be visible. The mean confidence interval for the interfacial stiffness flux parameter is ±1.3% of the fitted value, and the mean confidence interval for the attenuation coefficient is ±0.6% of the fitted value. As mentioned previously, the adhesive attenuation coefficient is known to decrease as a function of cure time. In addition to the bulk attenuation property, the phase responses show a monotonically increasing interfacial stiffness per unit area constant during the cure process, leveling off at the same time as bulk attenuation at ∼25 min of UV light exposure. Showing sensitivity to small interfacial quality changes during this cure-monitoring experiment suggests ultrasonic phase measurements around the lap joint's anti-resonance frequency may be able identify previously undetectable kissing bonds.

C. Post-cure ultrasonic and mechanical adhesive bonding evaluation

In the same manner as the cure-monitored joint described in Sec. IV B, the glass adherent phase response was subtracted from each bonded joint's phase response to obtain the phase response of the bondline, $\phi_{BL}^{meas}(f)$. The $\phi_{BL}^{meas}(f)$ curves were fitted to the theoretical model of ultrasonic interactions with bonded joints expressed in Eq. (8). The same set parameters in Table III were used in the curve-fitting model with the exception of bondline thickness, which was measured for each specimen individually. Again, the adhesive sound velocity was set for each UV-exposure time from the measurement results discussed in Sec. IV A. The free parameters shown in Table IV including the same initial

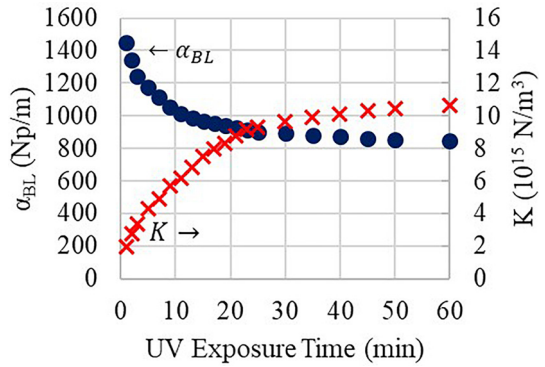

FIG. 8. (Color online) Adhesive attenuation coefficient (α_{adh}) and interfacial stiffness flux (K) vs UV exposure time, extracted from curve-fitting phase of bondline reflections.

guesses, lower bounds, and upper bounds were changed by the curve-fitting algorithm to find the theoretical curve which most closely matched the measured curve. For each bonded joint, the adhesive attenuation and interfacial stiffness flux constant were extracted, but the interfacial stiffness flux is the parameter of primary interest in this work.

From mechanical testing, the tensile strength of each bonded joint is determined by dividing the maximum load by the adhesive cross-sectional area. The tensile strength of each of the ten bonded joints is plotted as a function of UV-light exposure time in Fig. 9(a). Notably, each joint broke adhesively at one of the adhesive/adherent interfaces, regardless of tensile strength.

Similar to the attenuation and interfacial stiffness curves from the cure-monitored bonded joint in Fig. 8, the tensile strength of the lap joints levels off after about 25 min of UV light exposure. Since all lap joints failed at the adhesive/adherent interface, correlation of the ultrasonically measured interfacial stiffness flux constants with mechanically measured tensile strength was performed. The measured tensile strength vs interfacial stiffness flux of each bonded joint is plotted in Fig. 9(b).

According to results of Cantrell in epoxy/alumina bonds, the ultrasonic interfacial stiffness flux constant has a linear relationship with tensile strength.[7] The linear fit of the experimental tensile strength vs interfacial stiffness from this work shows this relationship holds true in Borofloat/NOA 60 bonded joints, as well. The strong correlation between ultrasonically measured interfacial stiffness and mechanical bond strength suggests swept-frequency phase measurements have sufficient sensitivity to predict interfacial bond quality.

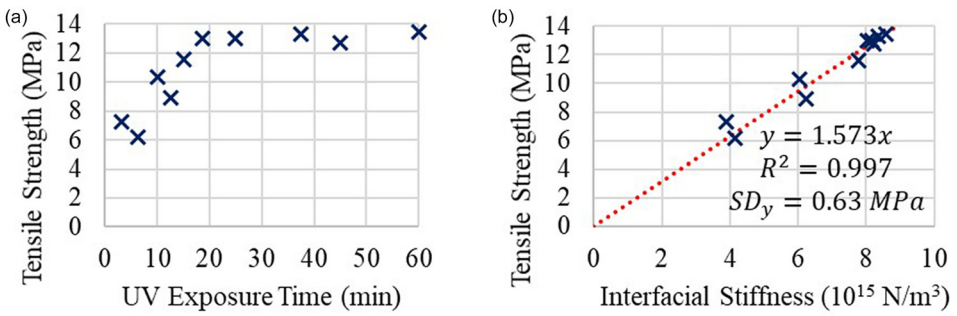

FIG. 9. (Color online) (a) Measured tensile strength as a function of UV light exposure; (b) Measured tensile strength vs interfacial stiffness flux for Borofloat/NOA 60/Borofloat tri-layer joints, including linear fit.

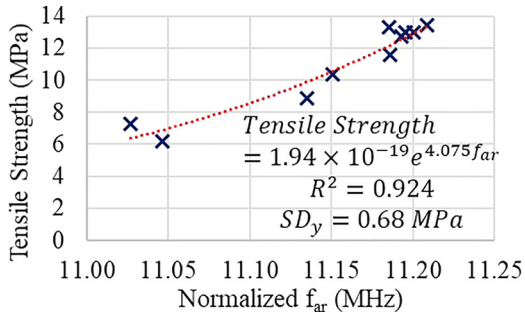

FIG. 10. (Color online) Tensile strength vs normalized anti-resonance frequency approximated from zero-crossing frequency of $\phi_{BL}^{meas}(f)$.

D. Single phase parameter correlation to tensile strength

To aid in speed and simplicity of interfacial bond quality evaluation, an additional method of using a single measured parameter from the measured phase spectrum was studied for its ability correlation to interfacial bond strength. Without using a curve-fitting method to solve the inverse problem of finding K from the measured phase spectrum, the anti-resonance frequency is correlated to tensile strength, directly.

In this study, the anti-resonance frequency of the bondline reflection coefficient is approximated by the zero-crossing frequency of the measured bondline phase response. That is, the zero-crossing frequency measured phase spectrum is the frequency at which $\phi_{BL}^{meas}(f_{ar}) = 0\,\text{deg}$. For a perfect bonded joint, $f_{ar} = c_{adh}/2L_{BL}$, but weak interfacial stiffness causes a reduction in anti-resonance frequency. Figure 10 displays the tensile strength vs the anti-resonance frequency from the phase response of each joint after normalization to the nominal thickness of 102 μm and fully cured sound velocity of 2316 m/s. The normalization of anti-resonance frequency factors out sound velocity changes as a function of degree-of-cure as well as bondline thickness variations, leaving only anti-resonance shifts due to interfacial stiffness. In Fig. 10, a strong exponential correlation between tensile strength and normalized anti-resonance frequency is observed. Given a normalized anti-resonance frequency measurement, ultimate tensile strength is predicted by the exponential curve fit within a standard deviation of 0.23 MPa. Such a curve fit is unique for a given bonded joint configuration. This indicates interfacial bond strength may be predicted by the zero-crossing frequency of the ultrasonic phase response of a bonded joint.

V. CONCLUSION

Analysis of swept-frequency ultrasonic phase measurements of bondline reflections in glass/UV-curable adhesive tri-layer bonded joints have been shown able to quantitatively assess adhesive bonding properties without the presence of interfacial contamination or gross bonding defects. This method uses commercial ultrasonic transducers with CFPPLL technology to obtain high-resolution ultrasonic phase measurements of ultrasonic tone-burst reflections over a selectable range of frequencies. Narrowband filtering of the measured tone-burst promotes noise suppression and higher signal-to-noise ratio, resulting in lower phase measurement uncertainty.

By focusing on the phase response near the ultrasonic anti-resonance frequency of the bondline reflection coefficient, the shift in anti-resonance frequency is measured as a function of adhesive cure. The adhesive stiffness and resulting sound velocity change during cure is measured separately via broadband ultrasound ToF. After curve-fitting to the theoretical ultrasonic interaction with imperfectly bonded joints, the attenuation coefficient as well as the interfacial stiffness flux are extracted. The correlation to mechanical tensile strength is consistent with the theoretical linear relationship between interfacial stiffness and absolute interfacial bond strength. In this work, interfacial bond strength is predicted by interfacial stiffness flux to a standard deviation of 0.63 MPa. As such, the swept-frequency ultrasonic phase method identified intermediate adhesion strengths, rather than simply identifying good or bad bonds. The demonstrated swept-frequency phase method is compatible with conventional ultrasonic transducers and inspection setups, while not suffering from amplitude-based sources of uncertainty, such as adherent attenuation differences and surface roughness.

Future work will investigate real-world bonded structures, where contamination can unknowingly reduce adhesion quality, and will study the ability of swept-frequency phase measurements to not only detect kissing bonds but also quantitatively measure interfacial bond strength. In cases where the adhesive cure cycle is well-controlled so the adhesive sound velocity and attenuation coefficient are known constants, separate broadband ultrasonic ToF sound velocity measurements will not be necessary. The measurement technique and analysis demonstrate the applicability of the swept-frequency ultrasonic phase method for the NDE of interface quality in bonded joints.

ACKNOWLEDGMENTS

The authors would like to thank Russell Wincheski for his help in mechanically testing the bonded joints. This work was supported by a NASA Space Technology Research Fellowship and the Langley Professor Program.

[1]R. D. Adams and B. W. Drinkwater, "Nondestructive testing of adhesively-bonded joints," NDT&E Int. **30**(2), 93–98 (1997).
[2]P. Cawley, T. Pialucha, and M. Lowe, "A comparison of different methods for the detection of a weak adhesive/adhered interface in bonded joints," in *Review of Progress in Quantitative Nondestructive Evaluation* (Springer, Boston, 1993), Vol. 12, pp. 1531–1538.
[3]G. M. Light and H. Kwun, "Nondestructive evaluation of adhesive bond quality: State-of-the-art review," Nondestructive Testing Information Analysis Center, 1989.
[4]B. Ehrhart, B. Valeske, C.-E. Muller, and C. Bockenheimer, "Methods for the quality assessment of adhesive bonded CFRP structures—A resume," in *2nd International Symposium on NDT in Aerospace*, 2010.
[5]H. G. Tattersall, "The ultrasonic pulse-echo technique as applied to adhesion testing," J. Phys. D: Appl. Phys. **6**, 819–832 (1973).
[6]J.-M. Baik and R. B. Thompson, "Ultrasonic scattering from imperfect interfaces: A quasi-static model," J. Nondestr. Eval. **4**(3/4), 177–196 (1984).
[7]J. H. Cantrell, "Determination of absolute bond strength from hydroxyl groups at oxidized aluminum-epoxy interfaces by angle beam ultrasonic spectroscopy," J. Appl. Phys. **96**(7), 3775–3781 (2004).

[8]J. H. Cantrell, "Hydrogen bonds, interfacial stiffness moduli, and the interlaminar shear strength of carbon fiber-epoxy matrix composites," AIP Adv. **5**, 037125 (2015).
[9]J. Cantrell, "Assessment of adhesive bond strength from ultrasonic tone-bursts," J. Nondestr. Eval. **37**, 81 (2018).
[10]A. I. Lavrentyev and S. I. Rokhlin, "Determination of elastic moduli, density, attenuation, and thickness of a layer using ultrasonic spectroscopy at two angles," J. Acoust. Soc. Am. **102**(6), 3467–6477 (1997).
[11]S. I. Rokhlin, L. Wang, B. Xie, V. A. Yakovlev, and L. Adler, "Modulated angle beam ultrasonic spectroscopy for evaluation of imperfect interfaces and adhesive bonds," Ultrasonics **42**, 1037–1047 (2004).
[12]P. B. Nagy, "Ultrasonic detection of kissing bonds at adhesive interfaces," J. Adhes. Sci. Technol. **5**(8), 619–630 (1991).
[13]C. Gauthier, M. E.-C. El-Kettani, J. Galy, M. Predoi, D. Leduc, and J.-L. Izbicki, "Lamb wave characterization of adhesion levels in aluminum/epoxy bi-layers with different cohesive and adhesive properties," Int. J. Adhes. Adhes. **74**, 15–20 (2017).
[14]M. Castaings, "SH ultrasonic guided waves for the evaluation of interfacial adhesion," Ultrasonics **54**(7), 1760–1775 (2014).
[15]D. Yan, B. W. Drinkwater, and S. A. Neild, "Measurement of the ultrasonic nonlinearity of kissing bonds in adhesive joints," NDT&E Int. **42**, 459–466 (2009).
[16]R. J. Freemantle and R. E. Challis, "Combined compression and shear wave ultrasonic measurements on curing adhesive," Meas. Sci. Technol. **9**(8), 1291–1302 (1998).
[17]E. Siryabe, M. Renier, A. Mezaine, J. Galy, and M. Castaings, "Apparent anisotropy of adhesive bonds with weak adhesion and non-destructive evaluation of interfacial properties," Ultrasonics **79**, 34–51 (2017).
[18]R. S. Dwyer-Joyce, "The application of ultrasonic NDT techniques in tribology," Proc. Inst. Mech. Eng., Part J: J. Eng. Tribol. **219**(5), 347–366 (2005).
[19]S. Mezil, F. Bruno, S. Raetz, J. Laurent, D. Royer, and C. Prada, "Investigation of interfacial stiffness of a tri-layer using zero-group velocity Lamb modes," J. Acoust. Soc. Am. **138**(5), 3202–3209 (2015).
[20]A. Baltazar, L. Wang, B. Xie, and S. I. Rokhlin, "Inverse ultrasonic determination of imperfect interfaces and bulk properties of a layer between two solids," J. Acoust. Soc. Am. **114**(3), 1424–1434 (2003).
[21]S. Biwa, S. Hiraiwa, and E. Matsumoto, "Stiffness evaluation of contacting surfaces by bulk and interface waves," Ultrasonics **47**(1–4), 123–129 (2007).
[22]J. Krolikowski and J. Szczepek, "Phase Shift of the reflection coefficient of ultrasonic waves in the study of the contact interface," Wear **157**, 51–64 (1992).
[23]K. Milne, P. Cawley, P. B. Nagy, D. C. Wright, and A. Dunhill, "Ultrasonic non-destructive evaluation of titanium diffusion bonds," J. Nondestr. Eval. **30**, 225–236 (2011).
[24]E. Escobar-Ruiz, D. C. Wright, I. J. Collison, P. Cawley, and P. B. Nagy, "Reflection phase measurements for ultrasonic NDE of titanium diffusion bonds," J. Nondestr. Eval. **33**, 535–546 (2014).
[25]T. Yilmaz, B. Ercikdi, K. Karaman, and G. Kulekci, "Assessment of strength properties of cemented paste backfill by ultrasonic pulse velocity test," Ultrasonics **54**(5), 1386–1394 (2014).
[26]R. L. V. Kumar, M. R. Bhat, and C. R. L. Murthy, "Some studies on evaluation of degradation in composite adhesive joints using ultrasonic techniques," Ultrasonics **53**, 1150–1162 (2013).
[27]A. Baudot, J. Moysan, C. Payan, N. Ylla, J. Galy, B. Verneret, and A. Baillard, "Improving adhesion strength analysis by the combination of ultrasonic and mechanical tests on single lap joints," J. Adhes. **90**(5–6), 555–568 (2014).
[28]L. Adler, S. Rokhlin, C. Mattei, G. Blaho, and Q. Xie, "Angle beam ultrasonic spectroscopy system for quantitative inspection of adhesive bonds," in *Review of Progress in Quantitative Nondestructive Evaluation* (Springer, Boston, 1999), Vol. 18, pp. 1553–1559.
[29]H. A. Haldren, D. F. Perey, W. T. Yost, K. E. Cramer, and M. C. Gupta, "A digital, constant-frequency pulsed phase-locked-loop instrument for real-time absolute ultrasonic phase measurements," Rev. Sci. Instrum. **89**, 054902 (2018).
[30]L. E. Kinsler, A. R. Frey, A. B. Coppens, and J. V. Sanders, "Tables of physical properties of matter," in *Fundamentals of Acoustics* (Wiley, New York, 2000), pp. 526–528.